

## INCLUSION AND CHARACTERIZATION OF KETOPROFEN INTO DIFFERENT MESOPOROUS SILICA NANOPARTICLES USING THREE LOADING METHODS

A. ABD-ELBARY<sup>1</sup>, M. A. EL NABARAWI <sup>1\*</sup>, D. H. HASSEN<sup>2</sup>, A. A. TAHA<sup>2</sup>

<sup>1</sup>Department of Pharmaceutics and Industrial Pharmacy, Faculty of Pharmacy, Cairo University, Kasr El- Aini Street, Cairo 11562, Egypt,

<sup>2</sup>Department of Pharmaceutics and Industrial Pharmacy, College of Pharmacy, Misr University for Science and Technology (MUST), sixth of October city, Almotamayez District, Giza, Egypt.  
Email: nabrwima@hotmail.com

Received: 14 Jun 2014 Revised and Accepted: 20 Aug 2014

### ABSTRACT

**Objective:** The objective of the present study was to encapsulate ketoprofen into MCM-41, SBA-15 and uncalcined SBA-15 (unc SBA-15) using different loading methods. Investigate the effect of using different loading methods, and the effect of pore sizes on the loading capacity of mesoporous silica. Finally, determine if any changes in the mesoporous structure occurred after KP loading.

**Methods:** Ketoprofen (KP) with about 1.5 nm molecular size was selected for encapsulation into three mesoporous silica nanoparticles (MSN). These MSN particles were selected to cover a wide range of pore diameters: MCM-41 (3.4 nm), SBA-15 (6.2 nm) and uncalcined SBA-15 (7.0 nm). Loading of KP was done by three loading methods namely rotavapor, soaking, and immersion method. The loading capacity was examined via solvent extraction. Characterization of the loaded mesoporous silica nanoparticles was done by high resolution transmission electron microscopy (HRTEM), small angle X-ray diffraction (SAXRD), nitrogen adsorption/desorption isotherms, differential scanning calorimetry (DSC), and Fourier transform infrared (FT-IR) spectroscopy.

**Results:** KP was successfully encapsulated into MCM-41, SBA-15 and uncalcined SBA-15 without affecting the mesoporous structure. The loading process was done using three different loading methods. Rotavapor loading method yielded higher loading capacities compared to soaking and immersion method. Another important factor that affected the amount of loaded KP into MSN particles were the Pore sizes of the host particles. MCM-41, which had the smallest pore size, had the least amount of loaded drug. On the other hand, uncalcined SBA-15, which had the largest pore size, had the highest amount of loaded KP.

**Conclusion:** This study is a promising issue for the incorporation of KP into different mesoporous silica nanoparticles.

**Keywords:** Ketoprofen, Mesoporous silica nanoparticles, MCM-41, SBA-15, Uncalcined SBA-15, Loading methods.

### INTRODUCTION

The International Pure and Applied Chemistry (IUPAC) classified pore materials into three types: micropore material (< 2 nm), mesoporous material (2–50 nm) and macropore material (>50 nm). Nowadays, applications of the macroporous substances are limited owing to their low surface area and large non-uniform pores. On the contrary, numerous applications of micro- and mesoporous materials are applied due to their large surface area and uniform pore structure[1].

Silicon is the second abundant element in the earth's crust after oxygen. Silicon occurs as oxygen containing compound termed Silicon dioxide (SiO<sub>2</sub>) which is known as silica. The first mesoporous silicananoparticles (MSN) were developed by Mobil Oil Corporation (Mobil) scientists in 1992. This was named M41S series (the Mobil 41 Series), their pore diameters ranged from 15 Å and 100 Å [2, 3]. MSNs proved to be promising candidates as drug delivery systems, they can be used either to control the release rates or to enhance the solubility of active substances[4–6]. MCM-41 (Mobil Composition of Matter 41) is one of the members of M41S series. MCM-41 is characterized by uniform honeycomb structure with pore diameter that can be tailored from 20 to 100 Å. The first attempt to use MSNs as drug delivery system was done by Valet-Regi *et al*, where they successfully loaded ibuprofen into MCM-41[7]. SBA-15 was first reported by Zhao *et al*, at the University of California, Santa Barbara[8]. SBA is the abbreviation for Santa Barbara Amorphous; it is characterized by having two-dimensional hexagonal structure with pore diameters ranging from 46 to 300 Å.

Ketoprofen (KP) is non steroidal anti-inflammatory drug (NSAID) belongs to the propionic acid NSAID class; its name is 2-(3-benzoyl phenyl) propionic acid. KP is a nonselective cyclooxygenase (COX) inhibitor; it has analgesic, antipyretic and antiarthritic effect through

inhibiting the prostaglandin and leukotriene synthesis. KP has very strong anti-inflammatory effect which is more potent than ibuprofen, phenylbutazone and aspirin[9]. It is used in the treatment of rheumatoid arthritis, osteoarthritis as well as in mild and moderate pain. KP is suitable for incorporation into ordered mesoporous silica having particle size about 15.3Å as well as having a carboxylic acid group, which can form hydrogen bonding with the silanol in mesoporous silica.

The aim of this work is to encapsulate ketoprofen into MCM-41, SBA-15 (template occluded) and uncalcined SBA-15 using different loading methods.

### MATERIALS AND METHODS

#### Materials

Ketoprofen was obtained as a gift sample from (Egyptian International Pharmaceutical Industries Company, Cairo, Egypt), Cetyltrimethylammonium bromide (CTAB) and Tetraethyl orthosilicate (TEOS) was obtained from (Sigma Aldrich, St. Lewis, USA), Pluronic P123 (BASF GmbH, Ludwigshafen, Germany). Other reagents and solvents were of HPLC grade.

#### Methods

##### Synthesis of MCM-41

MCM-41 synthesis was performed according to a previous report[10]. About 0.46 g sodium hydroxide was completely dissolved in 120 ml deionized water with stirring. After the solution became clear, 1.4 g CTAB was added and dissolved completely, 5.6 ml TEOS was poured into the above solution under vigorous stirring. Stirring continued for 24 hours and then the mixture was heated at 80°C for 48 hours. The mixture was filtered to obtain solid silica

particles then dried at 100°C for 6 hours. The surfactant was removed by calcination at 550°C for 5 hours.

### Synthesis of SBA-15 and uncalcined SBA-15

SBA-15 and unc SBA-15 synthesis were performed according to a standard method [8]. About 6 g of pluronic P123 was dispersed in 45g of H<sub>2</sub>O, then 180 g of HCl (2 M) and 12.8g of tetraethyl orthosilicate (TEOS) was added to the mixture. This mixture stirred for 24 h at 40 °C and then heated at 100 °C for another 24 h under a static condition. The mesoporous materials were recovered by filtration, washed with water, and then air-dried at room temperature without any calcinations giving uncSBA-15. A part of this solid was calcined at 550°C for 6 h to remove the template, to form SBA-15.

### Ketoprofen loading

Ketoprofen loading was done by three methods. Rotavapor method was done by dissolving ketoprofen in ethanol in the concentration (200mg/ml) while protected from light. Appropriate amount of the mesoporous silica was added to form Drug-particle ratio of 1:1. This mixture was shaken for 2 hours in an incubator shaker then, the solvent was evaporated for 15 minutes under reduced pressure using rotavapor. The samples were left to dry under vacuum for 24 hours at room temperature. The loaded particles were named MCM<sub>krt</sub>, SBA<sub>krt</sub>, and unc SBA<sub>krt</sub> for loaded ketoprofen into MCM-41, SBA-15 and uncalcined SBA-15 by rotavapor method, respectively. Soaking method was done using the same concentrations of ketoprofen and mesoporous silica to yield a drug to mesoporous ratio of 1:1. Ketoprofen was dissolved in ethanol then; appropriate amount of the mesoporous silica was added while protected from light. The loading process was performed in closed container to prevent evaporation of ethanol throughout the total loading time (24 hours). Then, all the samples were vacuum filtered using a Büchner funnel with the filter flask attached to a water aspirator. The loaded particles were named MCM<sub>ksk</sub>, SBA<sub>ksk</sub>, and unc SBA<sub>ksk</sub> for loaded ketoprofen into MCM-41, SBA-15 and uncalcined SBA-15 by soaking method, respectively. Finally, immersion method was done by dissolving ketoprofen in ethanol (200mg/ml) then; appropriate amount of the mesoporous silica was added while protected from light. The mixture was brought to equilibrium overnight under gentle stirring in closed container using magnetic stirrer then, filtered by vacuum filtration. The loaded particles were named MCM<sub>kim</sub>, SBA<sub>kim</sub>, and unc SBA<sub>kim</sub> for loaded ketoprofen into MCM-41, SBA-15 and uncalcined SBA-15 by soaking method, respectively.

### Methods of sample characterization

High Resolution Transmission Electron Microscope (HRTEM) images for mesopores as well as the wall channels were recorded using (HRTEM) (Tecnai G20 Super twin double tilt, USA) operating at 200 kV. Small angle XRD patterns were recorded on (Scintage XDS 2000 diffractometer, USA). The scan rate was 0.02 deg/min, step size of 0.01°, and a 2θ range of 0.60 – 10.00°. The nitrogen adsorption-desorption isotherms and the structural parameters were recorded using Nitrogen Adsorption/Desorption analyzer (Nova 3200, USA). The nitrogen adsorption/desorption isotherms were measured at -196.15 °C. The specific surface areas of samples were calculated using the Brunauer-Emmett-Teller (BET) method [11]. The total pore volume was assessed using the t-plot method of Lippens and De Boer [12]. The pore size distribution was calculated from the adsorption branch of isotherm using the Barrett-Joyner-Halenda (BJH) method [13]. DSC thermograms were recorded by a differential scanning calorimeter (Q 600 SDT Simultaneous DSC-TGA, USA). The samples scanned by rising the temperature at a rate of 10°C/min over a range between 0 to 200°C. FT-IR analysis was done by Fourier Transformation Infra-Red Spectroscopy (Jasco FT/IR 460 plus, Japan). The scanning range was 400-4000 cm<sup>-1</sup> and the resolution was 4 cm<sup>-1</sup>.

### Ketoprofen quantification by extraction method

The amount of ketoprofen loaded was determined by extraction in ethanol. Accurately weighed 10 mg of each of the drug loaded mesoporous silica was extracted in 20 ml ethanol for 6 hours with

continuous stirring on magnetic stirrer. Then, the samples were centrifuged at 5000 rpm for 30 minutes. The supernatant was collected and the amount of drug was spectrophotometrically determined at 259.0 nm. Each analysis was carried out in triplicate.

## RESULTS AND DISCUSSION

### Characterization of mesoporous silica nanoparticles

The HRTEM images for the three mesoporous silica nanoparticles showed the regular hexagonal array (honeycomb pattern) characteristic for mesoporous materials (Figure 1).

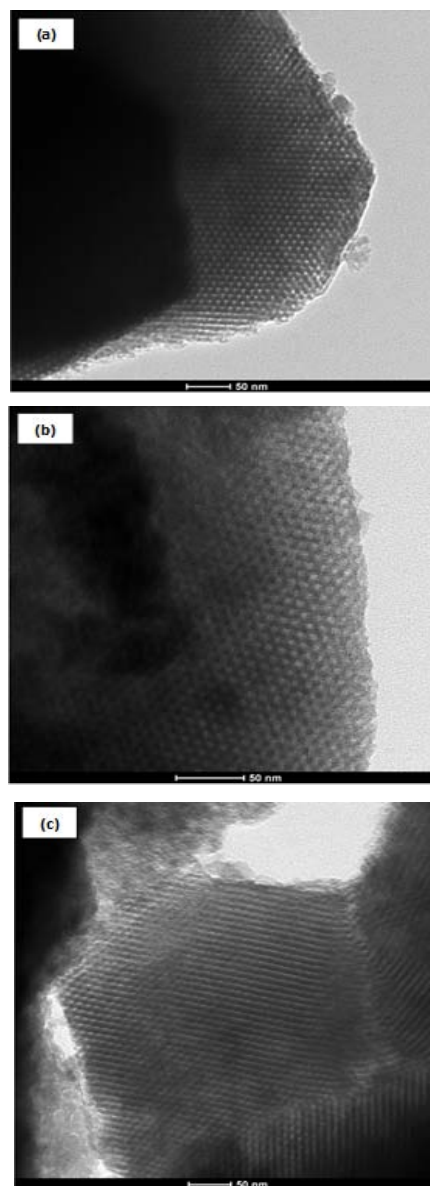


Fig. 1: HRTEM images of a) MCM-41, b) SBA-15, and c) unc SBA-15.

SAXRD patterns are shown in (Figure 2). MCM-41 ordered hexagonal array was further confirmed by the x-ray diffractogram, showing four Bragg reflections that can be indexed as (1 0 0), (1 1 0), (2 0 0) and (2 1 0) with the miller indices (hkl), where h, k, and l are integers, this reveals typical hexagonal *p6mm* configuration [14]. The 2θ diffraction angle was located at 2.2, 4.0, 4.6 and 5.5 degree, and the corresponding *d* spacing was 45.52, 25.93, 22.62 and 17.15 Å, respectively. The intense reflection that corresponded to the (1 0 0) diffraction peak with *d* spacing = 45.5 Å gave a lattice constant (cell parameter which is the distance from centers of two adjacent pores) of  $a_0 = 52.5 \text{ \AA}$  estimated by the hexagonal unit cell relation ( $a_0 = 2d_{100} / \sqrt{3}$ ) [15].

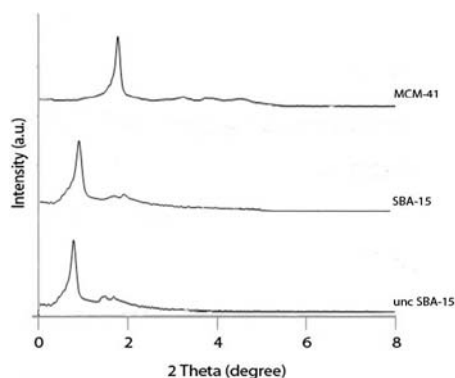


Fig. 2: SAXRD patterns for a) MCM-41, b) SBA-15, and c) unc SBA-15.

X-ray diffraction patterns of SBA-15 and unc SBA-15 denoted that both materials exhibited well resolved diffraction peaks showing a prominent peak at  $2\theta=0.8-1^\circ$  and two weak peaks around  $2\theta=1.5-2^\circ$ . These peaks can be indexed by (1 0 0), (1 1 0) and (2 0 0) reflections associated with  $p6mm$  hexagonal symmetry typical for SBA-15 materials [8, 16, 17]. The SAXRD pattern of the SBA-15 exhibited three well-resolved diffraction peaks at  $2\theta = 0.84, 1.55,$  and  $1.74$  degree, the corresponding  $d$  spacing was 95, 55, and  $47.7 \text{ \AA}$ , respectively. The  $2\theta$  diffraction angle for the unc SBA-15 was located at 0.86, 1.48, and 1.71 degree, respectively. The corresponding  $d$  spacing was 100, 60, and  $52 \text{ \AA}$ , respectively. The intense reflection that corresponded to the (1 0 0) diffraction peak for the SBA-15 and unc SBA-15 gave a lattice constant (cell parameter) of  $a_0 = 109$  and  $115 \text{ \AA}$ , respectively. It was clear that there was a decrease in the  $d$ -spacing in case of the calcined SBA-15 compared to the uncalcined. This was directly linked to the removal of the surfactant molecules used as template from the channels by calcination and subsequent condensation of silanol groups in the SBA-15 walls as reported by Kang et al [18] when studying the effect of calcination on MCM-41. However, intensities of XRD peaks for the calcined SBA-15 increased compared to the uncalcined. This increase was caused by siloxane condensation during the calcinations process, which improves the ordering of the mesopores [19].

The nitrogen adsorption/desorption isotherms for the three MSN particles are shown in (Figure 3). MCM-41 nitrogen ads/des isotherm is a typical IV isotherm of mesoporous materials with a step in the range of  $P/P_0 = 0.3-0.4$  and reversible nitrogen condensation steps, which is typical for the filling of mesoporous systems [14].

It was clear that, no hysteresis loop appeared in the isotherm graph. Numerous nitrogen adsorption studies showed that adsorption/desorption hysteresis loops do not appear at relative pressures below  $\approx 0.42$ . Such behavior was attributed to instability of the liquid nitrogen meniscus [20] which could be suggested as an explanation of the reversible nitrogen condensation steps observed for MCM-41 materials [21, 22]. Moreover, the absence of hysteresis loop indicated that all the MCM-41 particles contain pores smaller than 4 nm [23].

SBA-15 isotherm showed the typical IV isotherms, ideal for mesoporous molecular sieves [24]. The isotherms present H1 hysteresis loop, indicative of well defined cylindrical pores [24]. Subsequently, the capillary condensation step occurred in the range of 0.6-0.8 relative pressure, which is expected for SBA-15 materials. The position of this step were found at high relative pressure indicating the presence of large pore size (above 5 nm) [25]. In addition, the sharpness of the adsorption branches (located at a relative pressure from 0.6 to 0.8) indicates a narrow mesopore sizes distributions characteristic for a good quality SBA-15 [19].

Uncalcined SBA-15 adsorption isotherm exhibited nearly the same adsorption isotherm curve type IV with a H1 hysteresis loop as the calcined SBA-15. However, the capillary condensation step shifted to higher relative pressure about 0.2, indicating that uncalcined SBA-15 had somehow larger pore size than the calcined SBA-15.

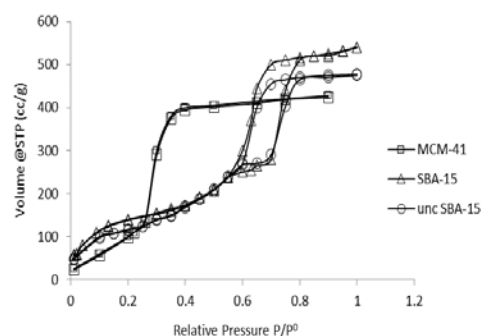


Fig. 3: Ads/des isotherms of MCM-41 (□), SBA-15 (Δ) and, unc SBA-15 (○).

Structural parameters (specific surface areas, total pore volume and average pore diameters) of different mesoporous nanoparticles were calculated from the adsorption isotherms (Table 1).

Table 1: Structural characterization of unloaded and loaded mesoporous nanoparticles

Formula	Specific Surface area (m <sup>2</sup> /g)	Total Pore Volume (cc/g)	Pore size (Pore diameter) (nm)	Particle size (μm)	Cell* Parameter a <sub>0</sub> (nm)	Wall** Thickness (nm)	Pore size distribution (nm)	Drug load (wt%)
MCM-41	920	1.2	3.46	1.5	5.25	1.85	13-21	-
MCM <sub>ksk</sub>	810	0.98	3.39	-	5.23	1.86	13-20	12.65±0.6
MCM <sub>kim</sub>	690	0.81	3.33	-	5.2	1.87	12-21	15.85±0.2
MCM <sub>krt</sub>	630	0.75	3.30	-	5.19	1.89	12-21	18.69±0.5
SBA-15	780	0.83	6.24	0.97	10.9	4.70	25-35	-
SBA <sub>ksk</sub>	700	0.78	6.20	-	10.9	4.70	24-33	19.82±0.3
SBA <sub>kim</sub>	680	0.69	6.11	-	10.9	4.79	23-32	28.42±0.7
SBA <sub>krt</sub>	653	0.65	6.05	-	10.9	4.85	22-32	33.00±0.1
unc SBA-15	820	1.04	7.03	1	11.5	4.50	28-40	-
unc SBA <sub>ksk</sub>	750	1.00	7.01	-	11.5	4.50	28-40	21.06±0.4
unc SBA <sub>kim</sub>	710	0.97	7.00	-	11.5	4.50	27-40	30.01±0.3
unc SBA <sub>krt</sub>	688	0.95	7.00	-	11.5	4.50	27-40	34.51±0.4

\*Cell parameter (a<sub>0</sub>) =  $2d_{100} / \sqrt{3}$ ; \*\*Wall thickness = a<sub>0</sub> - pore diameter

FT-IR spectra are shown in (Figure 4). MCM-41 infrared spectrum showed a stretching band at  $3400\text{ cm}^{-1}$  that is assigned to silanol groups linked to molecular water through hydrogen bonds with internal Si-OH groups. The broad band at  $1655\text{ cm}^{-1}$  is due to absorbed molecular water. Other bands were as follows:  $1100\text{ cm}^{-1}$  for Si-O-Si asymmetry stretching vibration,  $960\text{ cm}^{-1}$  for Si-O-H deformation,  $805\text{ cm}^{-1}$  for Si-O-Si symmetry stretching vibration and  $460\text{ cm}^{-1}$  for Si-O-Si bending vibration. The FT-IR spectroscopy showed the main peaks characteristic of the mesoporous silica network [26, 27].

FT-IR spectra of SBA-15 had broad bands of absorption at around  $3450\text{ cm}^{-1}$  corresponded to molecular water hydrogen bonded to each other and to Si-OH groups. They can be assigned to stretching vibrations of O-H and Si-OH bonds. The bands at around  $1620\text{ cm}^{-1}$  could be related to bending vibrations of O-H bonds in OH groups, overlapped with C-O-C stretching vibrations. The bands at around  $1080\text{ cm}^{-1}$  could be due to asymmetrical stretching vibrations of Si-O-Si, overlapped with Si-O-C, C-O-C and Si-C bond vibrations. The bands in  $980\text{-}950\text{ cm}^{-1}$  could be referred to stretching vibrations of free silanol (Si-OH) groups on the surface of the amorphous solid samples and C-O stretching vibration bonds are placed in this range. Symmetrical stretching vibrations of Si-O-Si bonds belonging to ring structures were observed around  $795\text{-}790\text{ cm}^{-1}$ . The bands in  $480\text{-}460\text{ cm}^{-1}$  could be assigned to associate Si-O-Si bond bending vibrations [28].

The uncalcined SBA-15 nearly had the same vibrational bands as the SBA-15. However, some differences to these bands appeared corresponding to the presence of the template triblock copolymer (Pluronic P 123). The broad band at about  $3440\text{ cm}^{-1}$  is partially due to the stretching vibrations of O-H and Si-OH bonds like in the calcined SBA-15 but also to C-H stretching attributed to presence of P123 in the uncalcined SBA-15. Furthermore, stretching bands in  $980\text{-}950\text{ cm}^{-1}$  are more intense compared to the calcined, which indicates that calcination decreases the number of silanol groups on the pore wall surfaces. On the other hand, new stretching bands appeared at  $2850\text{-}2930$ ,  $1350\text{-}1500$  originated from the vibrations of C-H, and at  $1110\text{ cm}^{-1}$  related to C-O-C vibration [29].

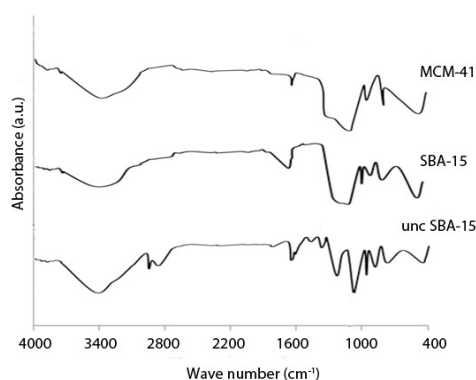


Fig. 4: FT-IR Spectra of MCM -41,SBA-15 and,unc SBA-15.

All the results concerning evaluation of the newly synthesized mesoporous silica confirmed that they belong to the ordered mesoporous silica materials.

#### Ketoprofen quantification

Table1 shows the amount of drug loaded (wt%) in different mesoporous silica corresponding to each loading method. As mentioned under the materials and method section, the drug-particle ratios were unified for all samples. Therefore, two factors affected the amount of loaded drug, the mesoporous silica nanoparticles type and the loading method. Regarding the mesoporous silica nanoparticles type, the amount of loaded KP increased in the following order: Unc SBA-15 >SBA-15 >MCM-41. Uncalcined SBA-15 had the largest pore size  $7\text{ nm}$  with surface area of  $820\text{ m}^2/\text{g}$  and  $1\text{ }\mu\text{m}$  particle size whereas, MCM-41 had the

smallest pore size  $3.4\text{ nm}$  with the highest surface area and particle size,  $920\text{ m}^2/\text{g}$  and  $1.5\text{ }\mu\text{m}$ , respectively. On the other hand, SBA-15 which came as second regarding the loading capacity had pore size of  $6.2\text{ nm}$  with the smallest surface area and particle size,  $780\text{ nm}$  and  $0.97\text{ }\mu\text{m}$  respectively. This would suggest that the surface area did not have a strong impact on the loading capacities meanwhile; pore sizes played a very crucial role in increasing the loading capacities of large size mesopores. Cauda et al [30] demonstrated that particles with larger pore diameter correlated with better loading efficiency. Conversely, mesoporous silica with small particle size has better loading capacities by shortening the diffusion length for the drug molecule [19, 31]. Therefore, both types of SBA-15 had higher loading capacities than MCM-41.

Concerning the loading method, it is clear that the amount of KP loaded was higher on using both immersion and rotavapor loading methods when compared to the amount loaded with soaking method. However, taking into consideration that loading KP by rotavapor method was performed nearly for two hours, while loading KP by immersion took 24 hours. This makes rotavapor method a very reliable and time preserving method. The key factor for high loading capacity is to keep the high concentration gradient of the drug in the solvent throughout the whole loading process. In rotavapor method, the diffusion and entrance of ketoprofen into the mesopores occur mainly during evaporation of the solvent, resulting in a high concentration gradient of the drug throughout the whole loading process. While in immersion method, the high concentration is present at the very beginning of the loading process. The drug diffusion and loading occur during stirring of the particles in the concentrated drug solution hence, the stirring maintained for 24hours. On the other hand, the soaking method did not provide a high concentration gradient because by time the concentration of the drug in the solvent will drop thus; there will be no driving force for the drug molecule to diffuse into to the mesoporous silica.

#### Characterization of Ketoprofen loaded Mesoporous Silica Nanoparticles

HRTEM images of KP loaded into MSN particles (Figure5) implied that all samples reserved the highly ordered honeycomb array structure. This showed that loading of KP did not affect the mesoporous internal structure.

SAXRD analysis for loaded KP into MCM-41 (Figure6A) showed that the hexagonal pore arrangement is not disrupted upon drug loading. The presence of intense (1 0 0) Miller indices reflection in the low  $2\theta$  region confirmed the preservation of the hexagonal structure corresponding to MCM-41 molecular sieve. However, the intensity of the peaks decreased with ketoprofen loading. Nevertheless, MCM-41 loaded with ketoprofen showed slight shifting in the positions of the (1 1 0), (2 0 0) and (2 1 0) peaks towards higher  $2\theta$  values; indicating decrease in the pore diameter of the MCM-41 when loaded with the drug [26]. The peaks shift and the decrease in peaks intensities were clearer with MCM<sub>krt</sub> sample owing to the higher KP loaded associated with rotavapor method (18.6 wt%). Moreover, on calculating the  $d$  spacing corresponding to the intense (1 0 0) diffraction peak for the loaded MCM-41, it was evident that some decrease in the  $d$  spacing values were detected. This decrease was again more obvious in MCM<sub>krt</sub> sample. The  $d$  spacing values decreased from  $4.55\text{ nm}$  for MCM-41 to  $4.5\text{ nm}$  for MCM<sub>krt</sub> sample. This decrease, consequently reflected on the cell parameters ( $a_0$ ) (Table1) of the loaded mesoporous silica, indicating that loading ketoprofen might result in MCM-41 molecular sieve host framework shrinkage [4].

Loaded SBA-15 samples diffractograms are represented in (Figure6B). The hexagonal pore arrangement was not disrupted upon drug loading showing well-defined peaks in the  $2\theta$  range of  $0.8$  to  $3^\circ$ , which match the patterns corresponding to the two-dimensional hexagonal symmetry ( $p6\text{ mm}$ ). SBA-15 loaded samples exhibited three well-resolved peaks related to (1 0 0), (1 1 0), and (2 0 0) planes. However, it should be noted that the intensity of diffraction patterns of loaded SBA-15 became weaker with shifting of the peaks to higher degrees corresponding to the increase in the amount of loaded KP i. e. SBA<sub>krt</sub> sample gave rise to more peak shift and decrease in peaks intensities. On the other hand, the  $d$  spacing

corresponding to the intense peak (1 0 0) diffraction for all the loaded samples were calculated. There were no significant changes

in the *d* spacing values, which means no cell parameter changes occurred after drug loading into the SBA-15.

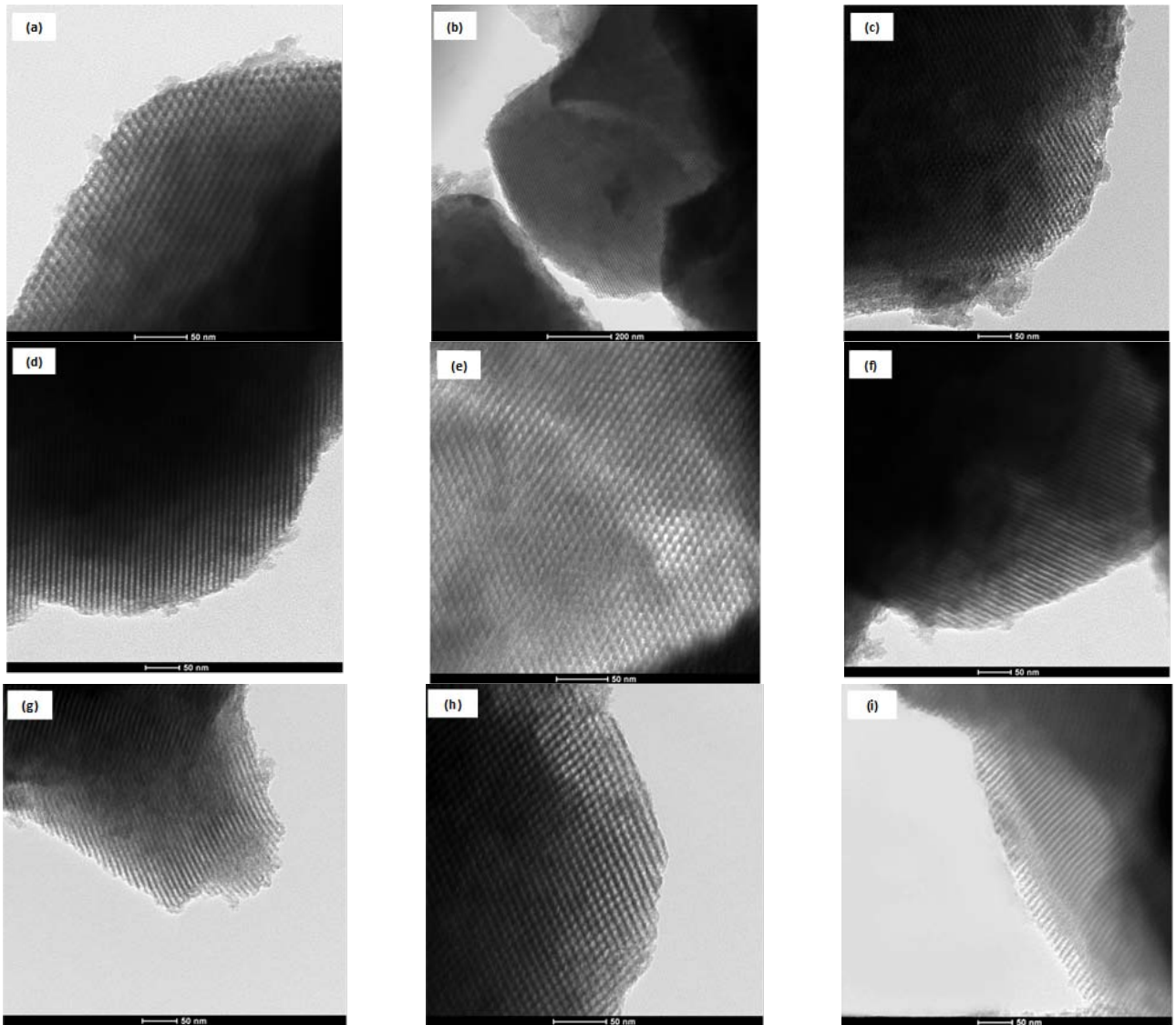


Fig. 5: HRTEM images of a) MCM<sub>ksk</sub>, b) MCM<sub>kim</sub>, c) MCM<sub>krt</sub>, d) SBA<sub>ksk</sub>, e) SBA<sub>kim</sub>, f) SBA<sub>krt</sub>, g) unc SBA<sub>ksk</sub>, h) unc SBA<sub>kim</sub>, and i) unc SBA<sub>krt</sub>.

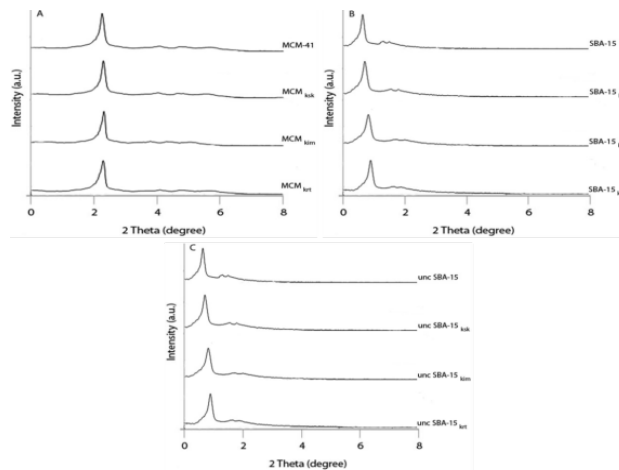


Fig. 6: SAXRD patterns of A: MCM-41, MCM<sub>ksk</sub>, MCM<sub>kim</sub>, MCM<sub>krt</sub>, B: SBA-15, SBA<sub>ksk</sub>, SBA<sub>kim</sub>, SBA<sub>krt</sub>, C: unc SBA-15, unc SBA<sub>ksk</sub>, unc SBA<sub>kim</sub>, and unc SBA<sub>krt</sub>.

Uncalcined SBA-15 loaded with KP exhibited three well-resolved peaks related to (1 0 0), (1 1 0), and (2 0 0) planes (Figure6C). It is clear that the hexagonal pore arrangement was not disrupted upon drug loading showing well-defined peaks in the  $2\theta$  range of 0.8 to 3°. Interestingly, unlike loaded MCM-41 and SBA-15 samples, loaded unc SBA-15 samples did not show peak shift either to lower or higher degrees. This different behavior is due to the presence of mesoporous template (triblock copolymer pluronic P123) in the uncalcined SBA-15. The surfactant chains disperse in the pores of the uncalcined SBA-15 like the spokes of the bicycle wheel providing a number of sub-nanometer (micropores) spaces and gaps for the drug to occupy [32]. Therefore, no changes in the pore channel sizes occurred.

Nitrogen ads/des isotherms for loaded MCM-41 samples exhibited typical IV isotherm of mesoporous materials with reversible

nitrogen condensation steps (Figure7A). This showed that after ketoprofen loading in MCM-41 molecular sieves; the characteristic mesoporous channel structure of MCM-41 did not destroy and still exist. The same results obtained with loaded samples into SBA-15, all samples exhibited typical IV isotherm (Figure7B).

The isotherms present a H1 hysteresis loop, indicative of well-defined cylindrical pores indicating that loading ketoprofen into the pores of SBA-15 did not affect its characteristic mesoporous channel structure. However, the capillary condensation pressures for loaded samples into MCM-41 and SBA-15 decreased; the adsorption/desorption isotherm branches shifted towards lower relative pressure. This shift was proportional to the amount of loaded KP, as the amount of loaded KP increase the shift to lower pressures increase as pore diameters becomes narrower.  $MCM_{krt} > MCM_{kim} > MCM_{ksk}$  similarly  $SBA_{krt} > SBA_{kim} > SBA_{ksk}$ .

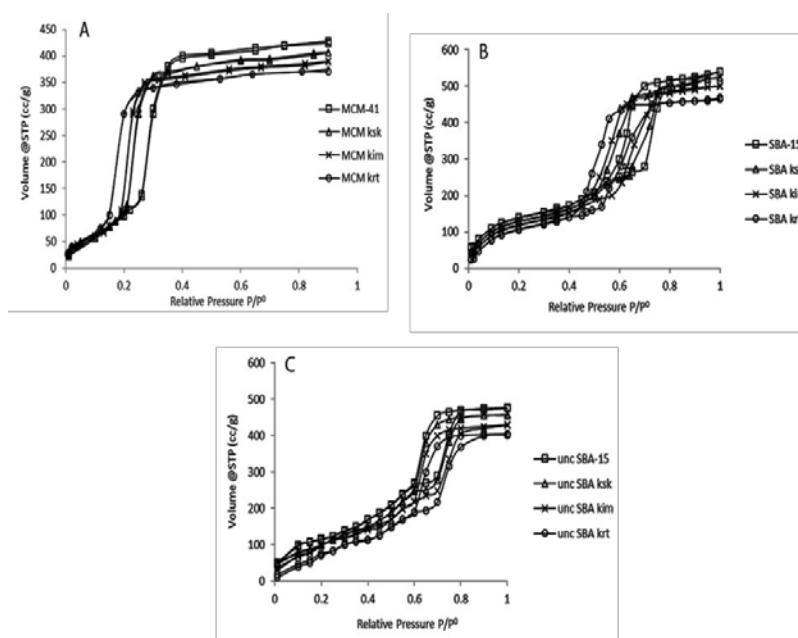


Fig. 7: Ads/des isotherms of A: MCM -41 (□), MCM<sub>ksk</sub> (Δ), MCM<sub>kim</sub> (×), MCM<sub>krt</sub> (○), B: SBA-15 (□), SBA<sub>ksk</sub> (Δ), SBA<sub>kim</sub> (×), SBA<sub>krt</sub> (○), C: unc SBA-15 (□), unc SBA<sub>ksk</sub> (Δ), unc SBA<sub>kim</sub> (×) and unc SBA<sub>krt</sub> (○).

Nitrogen ads/des isotherms for loaded unc SBA-15 showed a typical IV isotherm with H1 hysteresis loop (Figure7 C). Owing to the presence of P123 in the uncSBA-15, the ads/des isotherms for the loaded samples behaved differently from loaded MCM-41 and SBA-15 samples. The capillary condensation was nearly at the same relative pressures compared to the unloaded unc SBA-15. However, they showed slight decrease in the volume of nitrogen uptake, attributing to pore filling with ketoprofen.

On calculating, the specific surface areas and the total pore volumes for the loaded samples (Table 1), it was clear that all loaded samples showed decrease in specific surface areas and total pore volumes indicating the successful loading of KP. On the other hand, calculating the pore diameters for loaded KP into MCM-41 and SBA-15 showed decrease in the pore sizes. This decrease was proportional to the amount of loaded drug with respect to the loading method. Therefore, loaded KP in both MCM-41 and SBA-15 with rotavapor method (MCM<sub>krt</sub> and SBA<sub>krt</sub>) showed the strongest decrease in pore sizes as well as specific surface areas and total pore volumes. On the contrary, loaded unc SBA-15 revealed nearly no changes in the pore diameter they had diameter of 7 nm. However, the specific surface areas and total pore volumes decreased, indicating the successful loading of KP into unc SBA-15.

Furthermore, pore size distribution (PSD) curves for loaded samples into different MSN particles are shown in (Figure 8). All the

loaded samples showed uniform distribution curves indicating that loading of ketoprofen did not affect the mesoporous structure. Meanwhile, shifting of the distribution curves to the left (owing to the decrease in pore sizes) was observed with loaded samples into MCM-41 and SBA-15. These shifts reflected the difference in pore size diameters, which pointed to the effect of loading methods on the amount of loaded KP. On the other hand, pore size distribution curves of loaded unc SBA-15 did not show curve shifting, however there were decrease in the cumulative pore volumes.

FT-IR spectra for ketoprofen, unloaded and loaded MSN particles are shown in (Figure9). Ketoprofen spectrum showed a broad band at 3200 to 2500 cm<sup>-1</sup> due to O-H stretching and at 2970, 2930 cm<sup>-1</sup> due to C-H stretching of the methyl group. Moreover, there was a stretching band at 1695 cm<sup>-1</sup> due to C=O stretching vibration of the carboxylic group. Finally, there were different peaks in the fingerprint region below 1500 cm<sup>-1</sup> that confirm the racemic form of the drug[33]. As for the loaded samples, they showed characteristic peaks corresponding to the MSN particles whereas ketoprofen peaks did not appear. Furthermore, a new peak appeared at nearly 1730 cm<sup>-1</sup> due to hydrogen bonding of Si-OH (silanol group) with the COOH (carboxyl group) of KP indicating few interactions between carboxylic group and surface silanol group of MSN particles [7]. These results confirmed the successful encapsulation of KP into MSN particles pores with no evidence of surface adsorbed drug molecules.

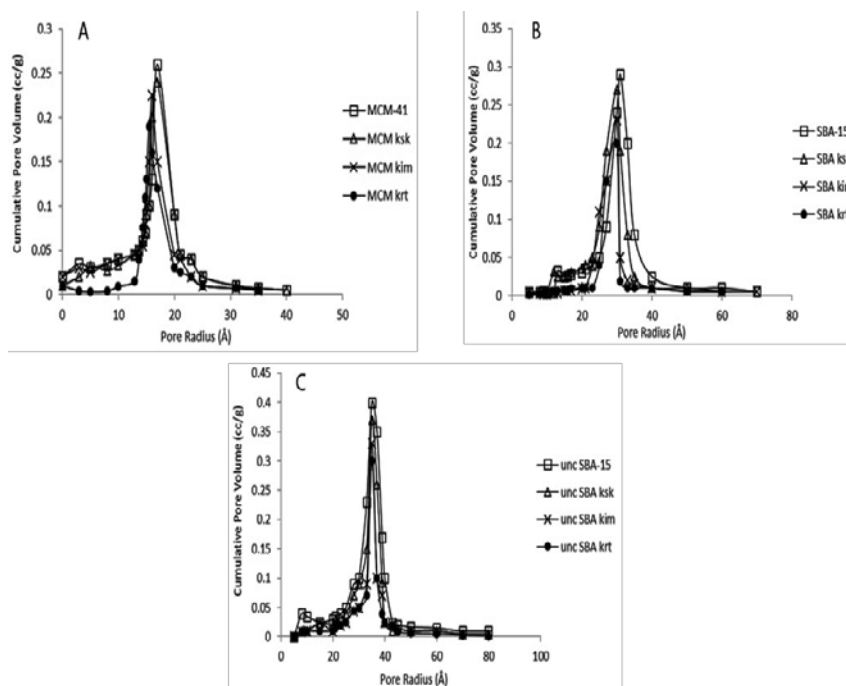


Fig. 8: Pore size distribution of A:MCM -41(□), MCM<sub>ksk</sub> (Δ), MCM<sub>kim</sub> (×), MCM<sub>krt</sub> (●),B: SBA-15(□),SBA<sub>ksk</sub> (Δ),SBA<sub>kim</sub> (×),SBA<sub>krt</sub> (●),C: unc SBA-15(□)unc SBA<sub>ksk</sub> (Δ), unc SBA<sub>kim</sub> (×) and unc SBA<sub>krt</sub> (●).

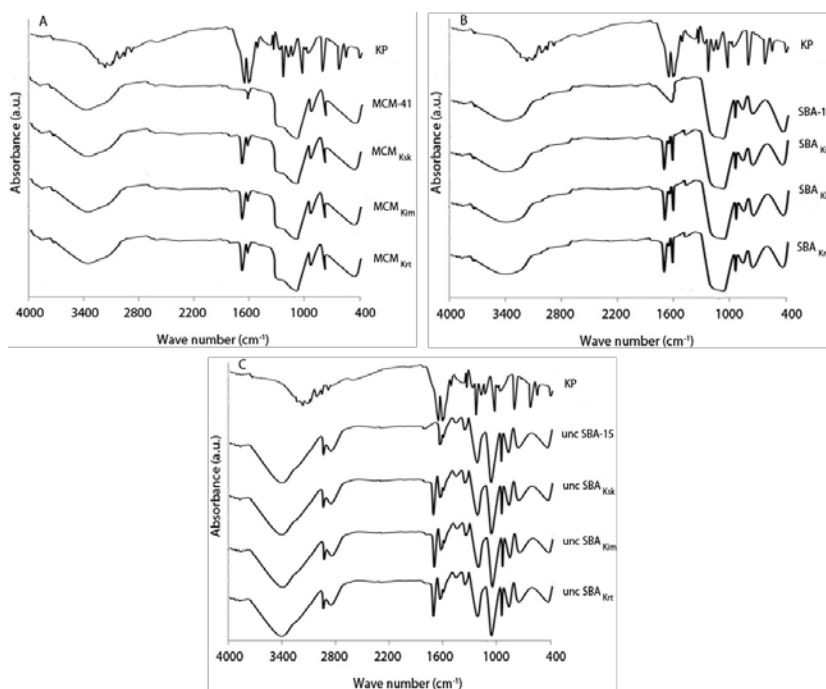
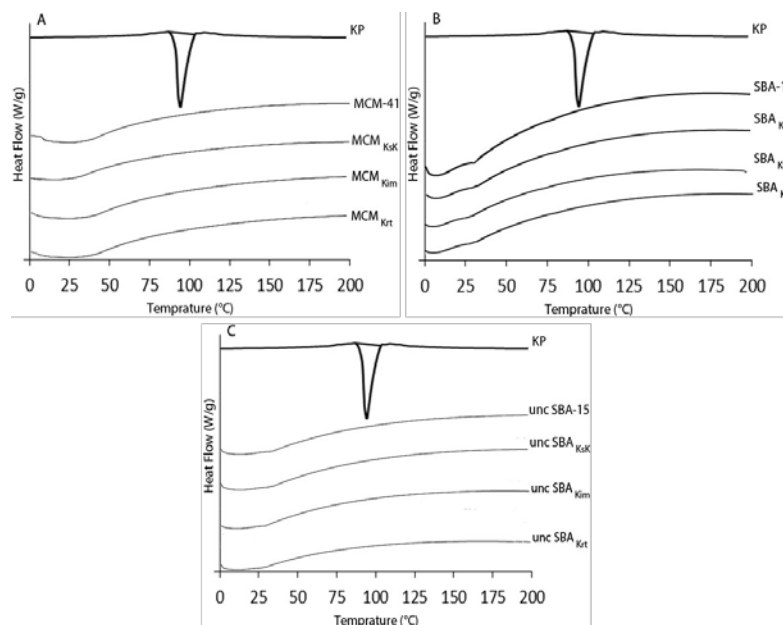


Fig. 9: Ft-IR spectra A: ketoprofen, MCM -41, MCM<sub>ksk</sub>, MCM<sub>kim</sub>, MCM<sub>krt</sub>, B: ketoprofen, SBA-15, SBA<sub>ksk</sub>, SBA<sub>kim</sub>, SBA<sub>krt</sub>, C: ketoprofen, uncSBA-15, unc SBA<sub>ksk</sub>, unc SBA<sub>kim</sub> and unc SBA<sub>krt</sub>.

The DSC thermogram patterns of ketoprofen, unloaded and loaded MSN particles are shown in (Figure10). Ketoprofen exhibited a characteristic single sharp endothermic peak with an onset at 92.51°C and an endset at 97.37°C with a peak at 96.56 °C corresponding to its melting endotherm with enthalpy of fusion equals 175.01J/g. This result was in accordance with previous reported melting ranges for ketoprofen[34]. Unloaded MSN particles showed no sharp endothermic peaks confirming its amorphous

nature. However, a very broad endothermic peak nearly below 70°C was detected. This broad endothermic peak is corresponding to physically adsorbed water. All loaded samples had nearly the same thermograms corresponding to the MSN particles.

Moreover, the thermograms did not show any traces of the characteristic endothermic peak corresponding to the drug. Thus, no surface adsorption of drug particles occurred during the loading process.



**Fig. 10: DSC thermograms of A: ketoprofen, MCM -41, MCM<sub>ksk</sub>, MCM<sub>kim</sub>, MCM<sub>krt</sub>, B: ketoprofen, SBA-15, SBA<sub>ksk</sub>, SBA<sub>kim</sub>, SBA<sub>krt</sub>, C: ketoprofen, uncSBA-15, uncSBA<sub>ksk</sub>, uncSBA<sub>kim</sub> and uncSBA<sub>krt</sub>.**

## CONCLUSION

KP was successfully encapsulated in MCM-41, SBA-15 and uncalcined SBA-15 without affecting the mesoporous structure. The loading process was done using three different loading methods. Rotavapor loading method yielded higher loading capacities compared to soaking and immersion method. Another important factor that affected the amount of loaded KP into MSN particles was the Pore sizes of the host particles. MCM-41, which had the smallest pore size, had the least amount of loaded drug. On the other hand, uncalcined SBA-15, which had the largest pore size, had the highest amount of loaded KP.

## CONFLICT OF INTERESTS

Declared None

## ACKNOWLEDGMENT

The authors would like to thank Prof. Dr. El-Zeiny M. Ebeid of Tanta University and MUST University, for helping in mesoporous silicate synthesis.

## REFERENCES

- Vartuli JC, Shih SS, Kresge CT, Beck JS. Potential Applications for M41S type mesoporous molecular sieves. In: L Bonneviot, F Beland, C Danumah, S Giasson, Kaliaguine S, editors. *Studies in Surface Science and Catalysis*. Volume 117. Amsterdam: Elsevier; 1998. p. 13-21.
- Beck JS, Vartuli JC, Roth WJ, Leonowicz ME, Kresge CT, Schmitt KD, *et al.* A new family of mesoporous molecular sieves prepared with liquid crystal templates. *J of the American Chemical Society* 1992;114:10834-43.
- Kresge CT, Leonowicz ME, Roth WJ, Vartuli JC, Beck JS. Ordered mesoporous molecular sieves synthesized by a liquid-crystal template mechanism. *Nature* 1992;359:710-2.
- Zhai Q-Z. Preparation and controlled release of mesoporous MCM-41/propranolol hydrochloride composite drug. *J of Microencapsulation* 2013;30:173-80.
- Slowing, II, Vivero-Escoto JL, Wu CW, Lin VS. Mesoporous silica nanoparticles as controlled release drug delivery and gene transfection carriers. *Advanced Drug Delivery Rev* 2008;60:1278-88.
- Ambrogi V, Perioli L, Marmottini F, Giovagnoli S, Esposito M, Rossi C. Improvement of dissolution rate of piroxicam by inclusion into MCM-41 mesoporous silicate. *European journal of pharmaceutical sciences: official J of the Eur Federation for Pharm Sci* 2007;32:216-22.
- Vallet-Regi M, Rámila A, Del Real RP, Pérez-Pariente J. A New Property of MCM-41: Drug Delivery System. *Chemistry of Materials* 2001;13:308-11.
- Zhao D, Feng J, Huo Q, Melosh N, Fredrickson GH, Chmelka BF, *et al.* Triblock copolymer syntheses of mesoporous silica with periodic 50 to 300 angstrom pores. *Sci* 1998;279:548-52.
- Kantor TG. Ketoprofen: a review of its pharmacologic and clinical properties. *Pharmacotherapy* 1986;6:93-103.
- Al-Kady AS, Gaber M, Hussein MM, Ebeid el ZM. Nanostructure-loaded mesoporous silica for controlled release of coumarin derivatives: a novel testing of the hyperthermia effect. *Eur Jof Pharmaceutics and Biopharmaceutics: official Journal of Arbeitsgemeinschaft fur Pharmazeutische Verfahrenstechnik eV* 2011;77:66-74.
- Fagerlund G. Determination of specific surface by the BET method. *Mat Constr* 1973;6:239-45.
- De Boer JH, Lippens BC, Linsen BG, Broekhoff JCP, van den Heuvel A, Osinga TJ. The curve of multimolecular N<sub>2</sub>-adsorption. *J of Colloid and Interface Sci* 1966;21:405-14.
- Barrett E, Joyner L, Halenda P. The Determination of Pore Volume and Area Distributions in Porous Substances. I. Computations from Nitrogen Isotherms. *J Am Chem Soc* 1951;73:373-80.
- Patil A, Chirmade UN, Slipper I, Lamprou DA, Urquhart A. Encapsulation of water insoluble drugs in mesoporous silica nanoparticles using supercritical carbon dioxide. *J of Nanomedicine and Nanotechnology* 2011;02:1-8.
- Souza MJB, Araujo AS, Pedrosa AMG, Marinkovic BA, Jardim PM, Morgado Jr E. Textural features of highly ordered Al-MCM-41 molecular sieve studied by X-ray diffraction, nitrogen adsorption and transmission electron microscopy. *Materials Letters* 2006;60:2682-5.
- Wu S, Han Y, Zou Y-C, Song J-W, Zhao L, Di Y, *et al.* Synthesis of Heteroatom Substituted SBA-15 by the "pH-Adjusting" Method. *Chemistry of Materials* 2004;16:486-92.
- Li Y, Zhang W, Zhang L, Yang Q, Wei Z, Feng Z, *et al.* Direct Synthesis of Al-SBA -15 Mesoporous Materials via Hydrolysis-Controlled Approach. *The J of Physical Chemistry B* 2004;108:9739-44.
- Kang F, Wang Q, Xiang S. Synthesis of mesoporous Al-MCM-41 materials using metakaolin as aluminum source. *Materials Letters* 2005;59:1426-9.

19. Qu F, Zhu G, Huang S, Li S, Sun J, Zhang D, *et al.* Controlled release of Captopril by regulating the pore size and morphology of ordered mesoporous silica. *Microporous and Mesoporous Materials* 2006;92:1-9.
20. Gregg SJ, Sing KSW. Adsorption, surface area, and porosity. 2nd ed. London: Academic Press; 1991.
21. Branton PJ, Hall PG, Sing KSW. Physisorption of nitrogen and oxygen by MCM-41, a model mesoporous adsorbent. *J of the Chemical Society, Chemical Communications* 1993;0:1257-8.
22. Branton PJ, Hall PG, Sing KSW, Reichert H, Schuth F, Unger KK. Physisorption of argon, nitrogen and oxygen by MCM-41, a model mesoporous adsorbent. *J of the Chemical Society, Faraday Transactions* 1994;90:2965-7.
23. Schulz-Ekloff G, Rathousky J, Zukal A. Controlling of morphology and characterization of pore structure of ordered mesoporous silicas. *Microporous and Mesoporous Materials* 1999;27:273-85.
24. Lowell S, Shields JE, Thomas MA, Thommes M. Characterization of Porous Solids and Powders: Surface Area, Pore Size and Density. 4th ed. Dordrecht: Springer Netherlands; 2006.
25. Szegedi A, Popova M, Goshev I, Mihály J. Effect of amine functionalization of spherical MCM-41 and SBA-15 on controlled drug release. *J of Solid State Chemistry* 2011;184:1201-7.
26. Wu S, Song K, Guan J, Kan Q. Synthesis and characterization of super-microporous material with enhanced hydrothermal stability. *Bull Mater Sci* 2011;34:979-83.
27. Li XD, Zhai QZ. Characterization of methylated nanoscale MCM-41 material. *JICS* 2011;8:S1-S8.
28. Azimov F, Markova I, Stefanova V, Sharipov K. Synthesis and characterization of SBA-15 and Ti-SBA-15 nanoporous materials for DME catalysts. *J of the University of Chemical Technology and Metallurgy* 2012;47:333-40.
29. Tian B, Liu X, Yu C, Gao F, Luo Q, Xie S, *et al.* Microwave assisted template removal of siliceous porous materials. *Chemical Communications* 2002;0:1186-7.
30. Cauda V, Mühlstein L, Onida B, Bein T. Tuning drug uptake and release rates through different morphologies and pore diameters of confined mesoporous silica. *Microporous and Mesoporous Materials* 2009;118:435-42.
31. Cauda V, Onida B, Platschek B, Mühlstein L, Bein T. Large antibiotic molecule diffusion in confined mesoporous silica with controlled morphology. *J of Materials Chemistry* 2008;18:5888.
32. Yue MB, Chun Y, Cao Y, Dong X, Zhu JH. CO<sub>2</sub> Capture by As-Prepared SBA-15 with an Occluded Organic Template. *Advanced Functional Materials* 2006;16:1717-22.
33. Liversidge GG. Ketoprofen In: *Analytical Profiles of Drug Substances Volume 10*. In: Florey K, editor. London: Academic Press; 1981. p. 443-71.
34. Tița D, Fuliș A, Tița B. Thermal stability of ketoprofen—active substance and tablets. *J Therm Anal Calorim* 2011;105:501-8.